P-ρ-T measurements of H2O up to 260 GPa under laser-driven shock loading

T. Kimura, N. Ozaki, T. Sano, T. Okuchi, T. Sano, K. Shimizu, K. Miyanishi, T. Terai, T. Kakeshita, Y. Sakawa , and R. Kodama

Citation: The Journal of Chemical Physics **142**, 164504 (2015); doi: 10.1063/1.4919052
View online: http://dx.doi.org/10.1063/1.4919052
View Table of Contents: http://scitation.aip.org/content/aip/journal/jcp/142/16?ver=pdfcov
Published by the AIP Publishing

P-ρ-T measurements of H_2O up to 260 GPa under laser-driven shock loading

T. Kimura,[1,2] N. Ozaki,[2,3] T. Sano,[4] T. Okuchi,[5] T. Sano,[2] K. Shimizu,[6] K. Miyanishi,[2] T. Terai,[2] T. Kakeshita,[2] Y. Sakawa,[4] and R. Kodama[2,3]
[1]*Geodynamics Research Center, Ehime University, 2-5 Bunkyo-cho, Matsuyama, Ehime 790-8577, Japan*
[2]*Graduate School of Engineering, Osaka University, Suita, Osaka 565-0871, Japan*
[3]*Photon Pioneers Center, Osaka University, Suita, Osaka 565-0871, Japan*
[4]*Institute of Laser Engineering, Osaka University, Suita, Osaka 565-0871, Japan*
[5]*Institute for Study of the Earth's Interior, Okayama University, Misasa, Tottori 682-0193, Japan*
[6]*KYOKUGEN, Center for Science and Technology under Extreme Conditions, Osaka University, Toyonaka, Osaka 560-8531, Japan*

(Received 15 December 2014; accepted 13 April 2015; published online 23 April 2015)

Pressure, density, and temperature data for H_2O were obtained up to 260 GPa by using laser-driven shock compression technique. The shock compression technique combined with the diamond anvil cell was used to assess the equation of state models for the *P-ρ-T* conditions for both the principal Hugoniot and the off-Hugoniot states. The contrast between the models allowed for a clear assessment of the equation of state models. Our *P-ρ-T* data totally agree with those of the model based on quantum molecular dynamics calculations. These facts indicate that this model is adopted as the standard for modeling interior structures of Neptune, Uranus, and exoplanets in the liquid phase in the multi-Mbar range. © *2015 AIP Publishing LLC.* [http://dx.doi.org/10.1063/1.4919052]

I. INTRODUCTION

H_2O is thought to be one of the most abundant compounds in ice giants such as Neptune and Uranus (e.g., Ref. 1). Therefore, the equation of state (EOS) for H_2O is critical for understanding the formation and composition of these planets and their temperature and pressure distributions. The ANEOS[2] and SESAME models[3] and the model based on quantum molecular dynamics (QMD) calculations[4,5] have been employed for modeling the interior structure of the ice giants. Recent shock experiments reported that their pressure and density data of H_2O are in good agreement with those of the QMD based EOS model,[6] indicating that this model is most suitable for modeling H_2O in the ice giants.

The QMD model predicted that a superionic conductor of H_2O exists in the deep interior of the icy planets above ~100 GPa.[4,7] Superionic H_2O is an ionic solid system that has high ionic conductivity well below the melting temperature.[8] Whether H_2O is in the superionic or liquid state in the planetary interior is of great importance to understanding the source of the planetary magnetic field.[9,10] Although some experimental studies reported the existence of the superionic phase,[11,12] recent measurements of the melting temperature of H_2O above the superionic phase show low melting temperatures and a quite gentle melting curve compared with those of the QMD prediction,[13] which implies that H_2O should remain in the liquid state even at deep interior conditions. This discrepancy between experimental and theoretical studies suggests that the QMD based EOS model is disputable for modeling the planetary interior. Indeed, the comparison between data obtained from the shock experiments and the QMD based EOS did not even cover the temperature.[6] Furthermore, the disagreement in the temperature of the kink of the melting curve between those of the experiments and the QMD based EOS is noteworthy. In fact, the temperature difference (T = 1000–1500 K) is larger than that of pressure (P = 35–47 GPa).[7,11] Taking into account these facts, EOS measurements covering pressure, density, and temperature (*P-ρ-T*) at extremely high pressures and temperatures are essential.

The laser-driven shock compression technique is useful for generating high pressure and temperature conditions comparable to the deep interiors of Neptune and Uranus. However, simultaneous measurements of *P-ρ-T* are challenging, especially temperature, because this requires absolute intensity measurements unlike the determination of the pressure or the density. In this study, we performed laser-driven shock experiments for H_2O up to 260 GPa and determined temperature from measured reflectivity and thermal emission, along with pressure and density. We also achieved temperature conditions lower than the principal Hugoniot states, which are comparably close to the planetary isentropes, by using the precompression cell applied for laser shock experiments.[14] The dataset of the principal and the off Hugoniot states can clarify the most validated EOS model.

II. EXPERIMENTAL PROCEDURE

The experiments were performed on the GEKKO/HIPER (High Intensity Plasma Experimental Research) laser facility at the Institute of Laser Engineering, Osaka University. In the experiments, we used nine beams of the system at a wavelength of 351 nm. A temporal profile of the laser pulse

was approximately a square shape in time with a full width at half maximum (FWHM) of 2.5 ns and the rise and fall times of 100 ps each. The focal-spot diameter was 600 μm with a flat top profile. Kinoform phase plates were used to achieve a uniform irradiation pattern. Spatially averaged intensities were 3.2×10^{13} to 6.9×10^{13} W/cm^2.[15]

A line-imaging velocity interferometer system for any reflector (VISAR) measured a shock velocity and a reflectivity in the sample.[16,17] An injection-seeded, Q-switched YAG laser was used as a probe-light source (532 nm/10 ns FWHM) in the VISAR, which irradiated the rear side of the target. Two VISARs with different velocity sensitivities were used to avoid the 2π phase-shift ambiguity due to the shock velocity jump at material interfaces. The velocity sensitivities were 4.78 and 11.3 (or 17.1) (km/s)/fringe in the water at ambient pressure with a density of 0.998 g/cm^3. The shock temperatures were measured with a different diagnostic tool. It consisted of a streaked optical pyrometer (SOP)[18,19] for a wavelength of 455 nm with 38 nm bandwidth. Spatially and temporally resolved temperatures were obtained from the self-emission of the shock-compressed matter with the absolutely calibrated SOP.

Ultra-pure water was loaded in the precompression cell for the laser-driven shock experiments. The diamond cell increased the initial pressure of the sample between 0.51 and 0.58 GPa. The samples at ambient pressure were also enclosed in the same cell. A detailed description of the cell was provided in our previous paper.[14] The thicknesses of thin (drive laser side) and thick (diagnostic side) diamonds were between 100 and 250 μm and 1000 μm, respectively. The thickness of the sample chamber was between 70 and 165 μm. The drive side of the thin diamond was coated with a gold x-ray preheat shield and a polypropylene ablator. The thickness of the Au shield and the CH ablator was 1.5 μm and 30 μm, respectively. On the sample chamber side, a z-cut α quartz was placed on the diamond and used as a reference standard for the impedance matching measurement.[20,21] The quartz thickness was 35 or 65 μm. There was an aluminum flash coating on the drive laser side of the quartz plate to clarify the breakout timing from the thin diamond. The thickness of the Al was 100 or 300 nm. Both sides of the thick rear diamond have antireflection coatings so that the VISAR does not detect spurious reflections from the stationary interfaces during shock loading. Initial pressure (P_0) was measured via the ruby fluorescence method.[22] The determination accuracy of the P_0 is better than ±50 MPa. The initial density (ρ_0) and refractive index (n_0) were derived from the EOS model for water at ambient pressure.[23,24]

III. RESULTS AND DISCUSSION

Figure 1 shows a velocity record extracted from the VISAR velocimetry image (inset in the Fig. 1). The time zero (t = 0) represents the shock breakout time from the Al coating. Both the shocked quartz and water are reflected during the transit across their layers, indicating that they transform to electronic conductors and the shock fronts reflect the 532 nm probe laser light of the VISAR diagnostic. Thus, the shock velocities of quartz and water (U_s^Q and U_s^w) were measured directly from the VISAR fringe shifts. The transit distance

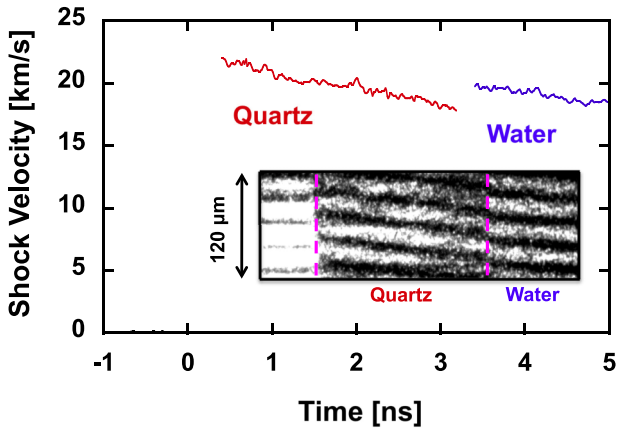

FIG. 1. Shock velocity in both quartz and water obtained from VISAR. The inset shows the corresponding raw VISAR image.

in both quartz and water determined from the time-integrated VISAR velocity is in agreement with the thicknesses measured before the experiments.

Figure 1 shows that the U_s^Q decays with time to a velocity of less than 80% of the maximum for ~2.5 ns. This velocity decay has to be taken into account for performing the impedance matching analysis (IMA). We adopted the U_s^Q and U_s^w immediately before and after the quartz–water interface for the IMA. A time gap found in the vicinity of where the shock transition from quartz to water was 70-150 ps, which is comparable to the temporal resolution of the streak camera of ~100 ps. To precisely determine the velocity at the interface time, we linearly fitted the velocities over 0.5 ns and extrapolated to forward or backward the impedance-matching time.[25] The velocities were calculated by averaging the shock profile over 100 ps. Here, we neglected the preheat effect, which was estimated to be less than 0.03 eV from radiation hydrodynamic simulations with the MULTI code.[26]

The particle velocity and pressure of quartz u_p^Q and P^Q were extracted from the measured U_s^Q and a Hugoniot U_s-u_p relation established by the Sandia Z-accelerator experiments; $U_s^Q = a + b\,u_p^Q - c\,u_p^Q e^{-du_p^Q}$, where $a = 6.26 \pm 0.35$ km/s, $b = 1.20 \mp 0.02$, $c = 2.56 \mp 0.15$, and $d = 0.37 \pm 0.02$ (km/s).[21] In order to determine H_2O Hugoniot states, the knowledge of the release isentrope for quartz is required. In this work, we used the inverted quartz Hugoniot as an approximation of the release isentrope. The IMA provides the Hugoniot state of water, the intersection of the quartz release curve, and the water Rayleigh line ($P = \rho_0^W U_s^W u_p$) in the P-u_p plane.[27]

The results of the EOS data for the water are listed in Table I. U_s^Q and U_s^W are direct experimental observables, which are obtained as a fringe shift at the image of the VISAR. The velocity uncertainty ≦1.5% was achieved because the fringe position was determined to ~4% of a fringe and the shock velocities measured here correspond to 3–4 fringes. P^W and ρ^W were determined from U_s^W and u_p^W using the Rankine-Hugoniot conservations.[27] The random errors for P^W and ρ^W arising from the measurement uncertainties were estimated with a Monte Carlo algorithm based on the assumption of Gaussian distribution about each observable.[28]

TABLE I. Principal and off-Hugoniot data for water. Random and systematic uncertainties are listed in parentheses (ran and sys). NP means normal (i.e., ambient) pressure.

Shot no.	$P_0{}^W$ (GPa)	$\rho_0{}^W$ (g/cm^3)	$U_s{}^Q$ (km/s)	$U_s{}^W$ (km/s)	$u_p{}^W$ (km/s)	P^W (GPa)	ρ^W (g/cm^3)
33522	NP	0.998	17.77 ± 0.19	19.83 ± 0.22	13.05 ± (0.22, 0.25)	258.2 ± (4.9, 4.9)	2.92 ± (0.12, 0.11)
33687	NP	0.998	13.88 ± 0.20	15.10 ± 0.23	9.58 ± (0.21, 0.35)	144.4 ± (3.6, 5.3)	2.74 ± (0.14, 0.19)
33679	0.53 ± 0.04	1.16 ± 0.01	16.62 ± 0.21	18.75 ± 0.23	11.51 ± (0.22, 0.28)	250.4 ± (5.4, 6.0)	3.00 ± (0.12, 0.12)
33696	0.58 ± 0.05	1.17 ± 0.01	13.05 ± 0.21	14.57 ± 0.23	8.47 ± (0.21, 0.37)	144.7 ± (3.9, 6.2)	2.79 ± (0.12, 0.19)
33705	0.51 ± 0.03	1.15 ± 0.01	14.42 ± 0.21	15.80 ± 0.23	9.69 ± (0.21, 0.34)	176.7 ± (4.2, 6.1)	2.98 ± (0.14, 0.17)

Total error includes systematic uncertainties in the quartz EOS used in the analysis as well as the measurement uncertainties and was estimated as a quadrature sum of both random and systematic uncertainties.

Figure 2(a) shows the principal Hugoniot plots in the P-ρ plane for water together with the results of the previous works[6,29–31] as well as the EOS models.[3–5] Estimated total uncertainties of the density in the present study are between 5.6% and 8.5%. The shock densities exhibit significant differences between the data of Knudson *et al.*[6] and Celliers *et al.*[29] in the intermediate region between the available gas-gun and the nuclear explosion experiments. The data obtained in this study are in good agreement with the data of Knudson *et al.*[6] rather than Celliers *et al.*[29] It is likely that the use of the aluminum step for IMA by Celliers *et al.*[29] gives a comparatively high density because the apparent shock velocity of the standard should be slightly faster due to averaging the shock profile in this step. Although our approximation of the release isentrope of the quartz is different from that of Knudson *et al.*,[6] their data agree well with our data within the error. Indeed, a density shift estimated based on an assumption that the release isentrope predicted by the QMD method has confidence is only ~2%,[32] which is small enough compared to the density error. Fig. 2(b) shows the off-Hugoniot states together with the data from Lee *et al.*[33] of which the initial pressures are close to 0.5 GPa (0.4 and 0.68 GPa) and the states predicted by the QMD and SESAME models.[3–5] The densities obtained in this study are lower than the data of Lee *et al.*[33] for the same reason as for the case of Celliers *et al.*,[29] as described above. Our data for both the principal and the off-Hugoniot states are in good agreement with those of the QMD based EOS model, as well as with the results of the measurements obtained by Knudson *et al.*[6]

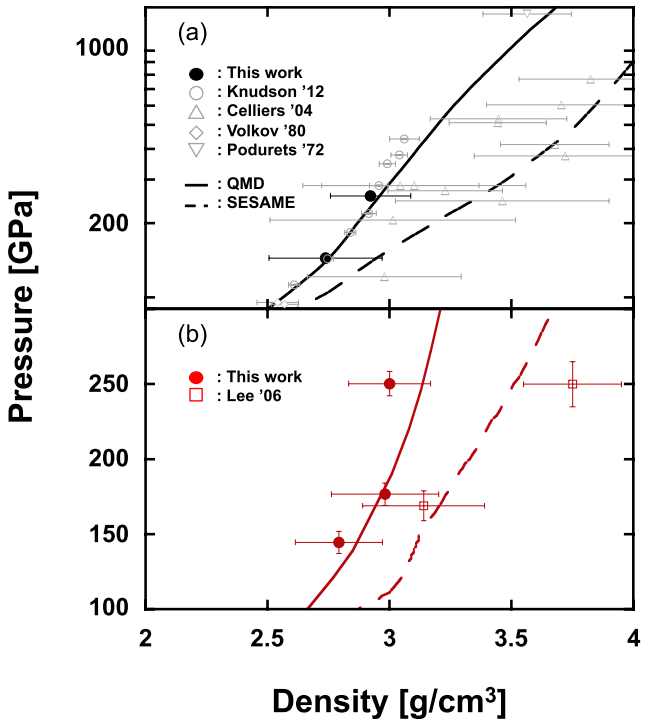

FIG. 2. (a) Principal Hugoniot plots in P-ρ plane for water. Data are from Celliers *et al.*[29] (triangle), Knudson *et al.*[6] (open circles), Volkov *et al.*[30] (diamonds), and this work (closed circles). Also, datum is from Podurets *et al.*[31] reanalyzed by Knudson *et al.*[6] using improved aluminum standard (inverted triangle). Also shown are the QMD based EOS model[4,5] (solid line) and SESAME model[3] (dashed line). (b) Off-Hugoniot plots obtained in this study (closed circles) together with data from *Lee et al.*[33] of which the initial pressures are near to 0.5 GPa (0.4 and 0.68 GPa) (open squares). Also shown are the EOS models same as in (a). Black and red colors represent the principal Hugoniot states and the off-Hugoniot states starting from 0.5 GPa, respectively.

The VISAR streak camera detected the intensities reflected from the observed shock fronts. In this work, the reflectivity of the shocked water was determined from the ratio of intensities just before and after the shock crossed the quartz–water interface.[34,35] The reflected intensity and the known reflectivity of quartz as a function of shock velocity provide the reflectivity of water.[34] The results of the reflectivity are listed in Table II. The total error includes measurement uncertainty and systematic uncertainty in quartz reflectivity. The reflectivities of the off-Hugoniot states are slightly lower than those of the principal Hugoniot, which indicate decreasing free carriers generated by thermal activation. The reflectivity data of the principal Hugoniot states are in good agreement with those of Knudson *et al.*,[6] as well as with the prediction from the QMD calculations of the Heyd, Scuseria, and Ernzerhof (HSE) exchange-correlation functional.[5]

The temperature T^W was measured using a SOP.[19] Recorded SOP intensities were modeled assuming a gray-body Planckian spectrum given by

$$I(\lambda,T) = \varepsilon(\lambda)\frac{2hc^2}{\lambda^5}\frac{1}{e^{hc/\lambda T}-1}, \quad (1)$$

where T is the temperature, ε is the emissivity, h is Planck's constant, and c is the speed of light. The emissivity is determined as $\varepsilon(\lambda) = 1 - R(\lambda)$, where $R(\lambda)$ is the reflectivity that is assumed to vary only slightly as a function of wavelength in the optical spectral range. We adopted the reflectivity at the VISAR wavelength assuming a weak dependence of R on the wavelength.[25] An example of the

TABLE II. Reflectivity and temperature data on the principal and the off-Hugoniot curves for water. The temperature of shot no. 33679 could not be estimated because the self-emission data were not obtained.

Shot no.	R^W (%)	T^W (10^3 K)
33522	24.0+4.0, −7.1	19.0+3.2, −3.3
33687	7.0+7.2, −3.8	9.6 ± 0.9
33679	17.3+5.1, −10.1	
33696	4.9+4.4, −2.9	7.2 ± 0.6
33705	8.2+3.8, −4.0	9.0 ± 0.9

emission intensity versus time data is shown in Fig. 3. The inset shows the raw image in the same shot. Clear intensity jumps are found in the aluminum–quartz and quartz–water interface. Shock arrival times in the interfaces from the SOP record are in agreement with those from the VISAR record. The temperature was obtained by averaging the profile of the time immediately after the quartz–water interface, over 170 ps corresponding to the temporal resolution of the streak camera.

The temperature results are listed in Table II. For shot no. 33679, the temperature could not be estimated because the self-emission data were not obtained. Estimated total uncertainty of the temperature is between 8% and 17%. This error arises from system calibration, measurements of self-emission, and the reflectivity of water. Taking into account changes in the optical property through the window due to, for instance, photo-excitation by low-level x-ray radiation generated by the ablation plasma,[34,36] we determined the sample temperature normalized to the quartz.[35] Fig. 4 shows the temperature data plotted against pressure together with the previous results[37] and Hugoniot curves predicted by the QMD based EOS and SESAME models. The temperatures of the off-Hugoniot states are significantly lower than those of the principal Hugoniot states, which is compatible with the reflectivity results. The difference in temperature between these two models significantly expands above 100 GPa. Our data of both the principal and the off-Hugoniot states are in very good agreement with those of the QMD based EOS, as well as the pressure and density results.

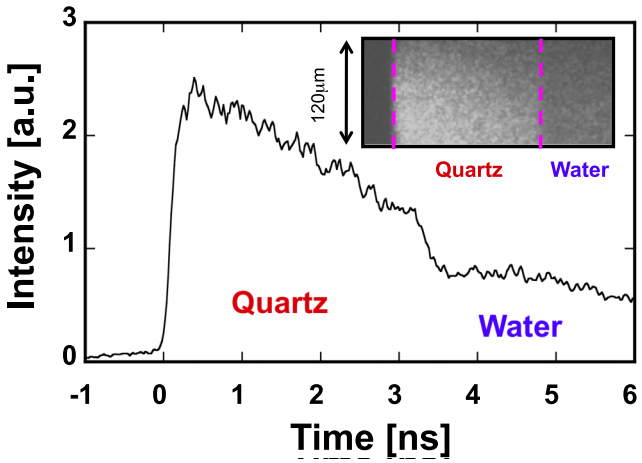

FIG. 3. Self-emission intensity in both quartz and water. The inset shows corresponding raw SOP image.

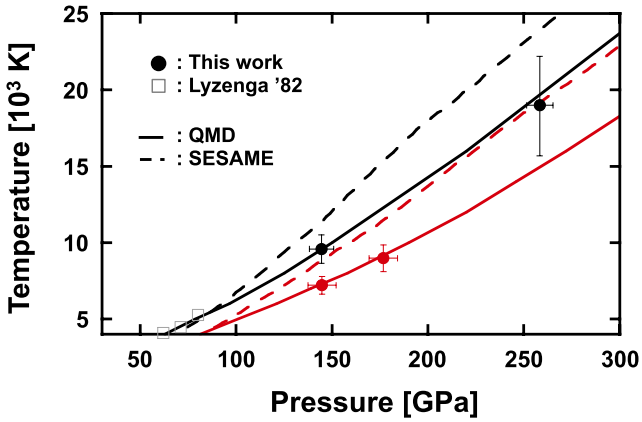

FIG. 4. Principal and off-Hugoniot data in P–T plane obtained in this study (closed circles) together with the previous results by Lyzenga *et al.*[37] (open squares). The temperature of shot no. 33679 could not be estimated because the self-emission data were not obtained. Also shown are the QMD based EOS model[4,5] (solid line) and SESAME model[3] (dashed line). Black and red colors represent the principal Hugoniot states and the off-Hugoniot states starting from 0.5 GPa, respectively.

Our data covering P-ρ-T agree well with those of the QMD based EOS. In addition, the QMD 300 K isotherm is also in good agreement with the measurements using diamond anvil cells.[38] Thus, the QMD model describes the EOS for water in solid and liquid states quite well. Moreover, the perfect agreement in reflectivity values between Knudson *et al.*,[6] the present experimental work shown here, and the QMD predictions[39] indicates that the QMD model reliably predicts electrical conductivity. The location of the superionic-to-plasma phase transition is important for understanding the dynamo source of Uranus and Neptune.[9,10] The boundary temperature estimated by the QMD calculation tends to be high compared with that obtained experimentally. For example, the predicted temperature at 70 GPa is about 2000 K,[7] on the other hand, the recent experimental study using a diamond anvil cell shows a lower temperature around 1400 K at 70 GPa.[13] A situation such as a disagreement in a melting curve though an agreement in EOS can happen since it is difficult to correlate EOS in the limited phases with the melting behavior. Especially, attention should be paid on the description for the melting from the superionic phase in which the proton has a high diffusivity. The phase transition in the QMD calculation is determined by observing the mean square displacements for oxygen ions.[4] Since melting can be thermodynamically defined in an approximate manner, the free energy comparison between solid and liquid states should be introduced in the QMD model in order to accurately determine the boundary (e.g., Ref. 40).

In addition to the fact that the experimental melting temperatures of H_2O are significantly lower than that of the QMD prediction,[13] the superionic-to-plasma phase boundary for the C–N–O–H mixture, which is a more realistic system for Uranus and Neptune, shifts downward.[41] Taking all of this into account, it is likely that the superionic ice is not present in deep interiors of their planets. Thus, the interior structure model including superionic ice is unrealistic.[10] Alternatively, the nonconvective layer in the deeper area of the icy region may be formed by a stable stratification due to the compositional

gradient.[1] The candidates as main components of the stratified layer can be C and N_2, according to some experimental studies[42–45] showing the dissociation of CH_4 and NH_3 at high pressures and temperatures. The precipitation and accretion of these heavier species may occur in the deeper region.

In summary, we have obtained P-ρ-T data for the EOS of not only the principal but also the off Hugoniot states up to 260 GPa. The dataset for the EOS on both the principal and the off Hugoniot curves is useful to assess the EOS models since it is possible to compare the states under the conditions that the contrast between the models clearly appears. We found that the QMD based model accurately describes the EOS for H_2O in the plasma phase along with the electrical property, while the location of superionic-to-plasma phase boundary is still disputable. Further work, such as EOS measurements of H_2O in the superionic phase are required for modeling the detailed structures of the icy giants as well as exoplanets. The laser-driven shock compression technique combined with the precompression cell allows us to approach such planetary internal conditions unreachable by conventional methods.

ACKNOWLEDGMENTS

We thank M. French for provision of the EOS of the off-principal Hugoniot where P_0 is 0.5 GPa and useful discussions about the *ab initio* calculations. We also thank Y. Hori, Y. Kuwayama, H. Dekura, Y. Tange, M. Nishi, and S. Whitaker for their helpful comments. We are deeply grateful to the GEKKO technical crew for their exceptional support during these experiments. This work was partially performed under the joint research project of the Institue of Laser Engineering, Osaka University. This work was supported by grants for the Global COE Program from the MEXT of Japan, and the CREST from JST. This work was also supported by grants from Grants-in-Aid for Scientific Research (Grant Nos. 25707041 and 22224012) and the Core-to-Core Program on International Alliance for Material Science in Extreme States with High Power Laser and XFEL of the Japan Society for the Promotion of Science.

[1]W. B. Hubbard, M. Podolak, and D. J. Stevenson, *The Interior of Neptune: Neptune and Triton* (University of Arizona Press, Tucson, 1995), pp. 109–138.
[2]S. P. Lyon and J. D. Johnson, Los Alamos Technical Report No. LA-UR-92-3407, 1992.
[3]National Technical Information Service Document No. DE94–011699 (J. D. Johnson, SESAME Tavles, 1994). Copies may be ordered from the National Technical Information Service, Springfield, VA 22161. For the water, we used SESAME Table 7150.
[4]M. French, T. R. Mattsson, N. Nettelmann, and R. Redmer, Phys. Rev. B **79**, 054107 (2009).
[5]M. French and R. Redmer, J. Phys.: Condens. Matter **21**, 375101 (2009).
[6]M. D. Knudson, M. P. Desjarlais, R. W. Lemke, T. R. Mattsson, M. French, N. Nettelmann, and R. Redmer, Phys. Rev. Lett. **108**, 091102 (2012).
[7]R. Redmer, T. R. Mattsson, N. Nettelmann, and M. French, Icarus **211**, 798 (2011).
[8]C. Cavazzoni, G. L. Chiarotti, S. Scandolo, E. Tosatti, M. Bernasconi, and M. Parrinello, Science **283**, 44 (1999).
[9]S. Stanley and J. Bloxham, Nature **428**, 151 (2004).
[10]B. Y. Tian and S. Stanley, Astrophys. J. **768**, 156 (2013).
[11]A. F. Goncharov, N. Goldman, L. E. Fried, J. C. Crowhurst, I. W. Kuo, C. J. Mundy, and J. M. Zaug, Phys. Rev. Lett. **94**, 125508 (2005).
[12]E. Sugimura, T. Komabayashi, K. Ohta, K. Hirose, Y. Ohishi, and L. S. Dubrovinsky, J. Chem. Phys. **137**, 194505 (2012).
[13]T. Kimura, T. Kuwayama, and T. Yagi, J. Chem. Phys. **140**, 074501 (2014).
[14]T. Kimura, N. Ozaki, T. Okuchi, T. Terai, T. Sano, K. Shimizu, T. Sano, M. Koenig, A. Hirose, T. Kakeshita, Y. Sakawa, and R. Kodama, Phys. Plasmas **17**, 054502 (2010).
[15]N. Ozaki, T. Sano, M. Ikoma, K. Shigemori, T. Kimura, K. Miyanishi, T. Vinci, F. H. Ree, H. Azechi, T. Endo, Y. Hironaka, Y. Hori, A. Iwamoto, T. Kadono, H. Nagatomo, M. Nakai, T. Norimatsu, T. Okuchi, K. Ohtani, T. Sakaiya, K. Shimizu, A. Shiroshita, A. Sunahara, H. Takahashi, and R. Kodama, Phys. Plasmas **16**, 062702 (2009).
[16]L. Barker and R. Hollenbach, J. Appl. Phys. **43**, 4669 (1972).
[17]P. M. Celliers, D. K. Bradley, G. W. Collins, D. G. Hicks, T. R. Boely, and W. J. Armstrong, Rev. Sci. Instrum. **75**, 4916 (2004).
[18]G. W. Collins, P. M. Celliers, L. B. Da Silva, R. Cauble, D. M. Gold, M. E. Foord, N. C. Holmes, B. A. Hammel, R. J. Wallace, and A. Ng, Phys. Rev. Lett. **87**, 165504 (2001).
[19]J. E. Miller, T. R. Boehly, A. Melchior, D. D. Meyerhofera, P. M. Celliers, J. H. Eggert, D. G. Hicks, C. M. Sorce, J. A. Oertel, and P. M. Emmel, Rev. Sci. Instrum. **78**, 034903 (2007).
[20]D. G. Hicks, T. R. Boehly, P. M. Celliers, J. H. Eggert, E. Vianello, D. D. Meyerhofer, and G. W. Collins, Phys. Plasmas **12**, 082702 (2005).
[21]M. D. Knudson and M. P. Desjarlais, Phys. Rev. Lett. **103**, 225501 (2009).
[22]H. K. Mao, P. M. Bell, J. W. Shaner, and D. J. Steinberg, J. Appl. Phys. **49**, 3276 (1978).
[23]W. Wagner and A. Pruß, J. Phys. Chem. Ref. Data **31**, 387 (2002).
[24]H. Shimizu, T. Nabetani, T. Nishiba, and S. Sasaki, Phys. Rev. B **53**, 6107 (1996).
[25]T. Sano, N. Ozaki, T. Sakaiya, K. Shigemori, M. Ikoma, T. Kimura, K. Miyanishi, T. Endo, A. Shiroshita, H. Takahashi, T. Jitsui, Y. Hori, Y. Hironaka, A. Iwamoto, T. Kadono, M. Nakai, T. Okuchi, K. Ohtani, K. Shimizu, T. Kondo, R. Kodama, and K. Mima, Phys. Rev. B **83**, 054117 (2011).
[26]R. Ramis, R. Schmalz, and J. Meyer-ter-Vehn, Comput. Phys. Commun. **49**, 475 (1988).
[27]Y. B. Zel'dovich and Y. P. Raizer, *Physics of Shock Waves and High—Temperature Hydrodynamic Phenomena* (Academic Press, New York, 1966).
[28]J. Eggert, S. Brygoo, P. Loubeyre, R. S. McWilliams, P. M. Celliers, D. G. Hicks, T. R. Boehly, R. Jeanloz, and G. W. Collins, Phys. Rev. Lett. **100**, 124503 (2008).
[29]P. M. Celliers, G. W. Collins, D. G. Hicks, M. Koenig, E. Henry, A. Benuzzi-Mounaix, D. Batani, D. K. Bradley, L. B. Da Silva, R. J. Wallace, S. J. Moon, J. H. Eggert, K. K. M. Lee, L. R. Benedetti, R. Jeanloz, I. Masclet, N. Dague, B. Marchet, M. Rabec le Gloahec, Ch. Reverdin, J. Pasley, O. Willi, D. Neely, and C. Danson, Phys. Plasmas **11**, L41 (2004).
[30]L. P. Volkov, N. P. Voloshin, R. A. Mangasarov, V. A. Simonenko, G. V. Sin'ko, and V. L. Sorokin, JETP Lett. **31**, 375 (1980).
[31]M. A. Podurets, G. V. Simakov, R. F. Trunin, L. V. Popov, and B. N. Moiseev, Sov. Phys. JETP **35**, 375 (1972).
[32]M. D. Knudson and M. P. Desjarlais, Phys. Rev. B **88**, 184107 (2013).
[33]K. K. M. Lee, L. R. Benedetti, R. Jeanloz, P. M. Celliers, J. H. eggert, D. G. Hicks, S. J. Moon, E. Henry, M. Koenig, and A. Benuzzi-Mounaix, J. Chem. Phys. **125**, 014701 (2006).
[34]P. M. Celliers, P. Loubeyre, J. H. Eggert, S. Brygoo, R. S. McWilliams, D. G. Hicks, T. R. Boehly, R. Jeanloz, and G. W. Collins, Phys. Rev. Lett. **104**, 184503 (2010).
[35]M. A. Barrios, D. G. Hicks, T. R. Boehly, D. E. Fratanduono, J. H. Eggert, P. M. Celliers, G. W. Collins, and D. D. Meyerhofer, Phys. Plasmas **17**, 056307 (2010).
[36]W. Theobald, J. E. Millerm, T. R. Boehly, E. Vianello, D. D. Meyerhofer, and T. C. Sangster, Phys. Plasmas **13**, 122702 (2006).
[37]G. A. Lyzenga, T. J. Ahrens, W. J. Nellis, and A. C. Mitchell, J. Chem. Phys. **76**, 12 (1982).
[38]E. Sugimura, T. Iitaka, K. Hirose, K. Kuwayama, N. Sata, and Y. Ohishi, Phys. Rev. B **77**, 214103 (2008).
[39]M. French, T. R. Mattsson, and R. Redmer, Phys. Rev. B **82**, 174108 (2010).
[40]L. Voadlo and D. Alfe, Phys. Rev. B **65**, 214105 (2002).
[41]R. Chau, S. Hamel, and W. Nellis, Nat. Commun. **2**, 203 (2010).
[42]L. R. Benedetti, J. H. Nguyen, W. A. Caldwell, H. Liu, M. Kruger, and R. Jeanloz, Science **286**, 100 (1999).
[43]H. Hirai, K. Konagai, T. Kawamura, Y. Yamamoto, and T. Yagi, Phys. Earth Planet. Inter. **174**, 242 (2009).
[44]S. S. Lobanov, P. N. Chen, X. J. Chen, C. S. Zha, K. D. Litasov, H. K. Mao, and A. F. Goncharov, Nat. Commun. **4**, 2446 (2013).
[45]J. G. O. Ojwang, R. S. McWilliams, X. Ke, and A. F. Goncharov, J. Chem. Phys. **137**, 064507 (2012).